Recent Changes in the Pacific Subtropical Cells Inferred from an Eddy-Resolving Ocean Circulation Model*

WEI CHENG

Joint Institute for the Study of the Atmosphere and Ocean, University of Washington, Seattle, Washington

MICHAEL J. MCPHADEN

Pacific Marine Environmental Laboratory, Seattle, Washington

DONGXIAO ZHANG

Joint Institute for the Study of the Atmosphere and Ocean, University of Washington, and Pacific Marine Environmental Laboratory, Seattle, Washington

E. JOSEPH METZGER

Naval Research Laboratory, Stennis Space Center, Mississippi

(Manuscript received 1 August 2005, in final form 8 August 2006)

ABSTRACT

In this study the subtropical cells (STC) in the Pacific Ocean are analyzed using an eddy-resolving ocean general circulation model driven by atmospheric forcing for the years 1992–2003. In particular, the authors seek to identify decadal changes in the STCs in the model and to compare them with observations in order to understand the consequences of such changes for the equatorial ocean heat and mass budgets. The simulation shows a trend toward increasing pycnocline volume transport at 9°N and 9°S across the basin from 1992 to 2003. This increase [4.9 ± 1.0 Sv (Sv ≡ 10^6 m^3 s^{-1})] is in qualitative agreement with observations and is attributed primarily to changes in the interior ocean transport, which are partially compensated by opposing western boundary transports. The subtropical meridional volume transport convergence anomalies in the model pycnocline are found to be consistent with anomalous volume transports in both the observed and modeled Equatorial Undercurrent, as well as with the magnitude of simulated anomalous upwelling transport at the base of the mixed layer in the eastern Pacific. As a result of the increased circulation intensity, heat transport divergence through the lateral boundaries of the tropical control volume (defined as the region between 9°N and 9°S, and from the surface to σ_θ = 25.3 isopycnal) increases, leading to a cooling of the tropical upper ocean despite the fact that net surface heat flux into the control volume has increased in the same time. As such, these results suggest that wind-driven changes in ocean transports associated with the subtropical cells play a central role in regulating tropical Pacific climate variability on decadal time scales.

1. Introduction

The subtropical cells (STCs) in the Pacific Ocean provide a mechanism for extratropical and tropical communication. This circulation is important for setting up the thermocline mean structure in the Tropics by subducting water in the subtropics and ventilating the equatorial ocean. As such, it can play a role in regulating tropical interannual climate variability since phenomena like El Niño are critically influenced by the structure of the mean background condition (e.g., Fedorov and Philander 2001). Recently variations in the STC have also been proposed as a possible mechanism for low-frequency climate variability (longer than interannual) in the Tropics. Gu and Philander (1997) suggest that decadal variations in equatorial sea surface temperature (SST) are influenced by the advection of water mass anomalies from the subtropics. Later stud-

---

Corresponding author address: Dr. Wei Cheng, Joint Institute for the Study of the Atmosphere and Ocean, University of Washington, Campus Box 357941, Seattle, WA 98115.
E-mail: wcheng@ocean.washington.edu

ies show that it is not evident that water mass anomalies generated at subtropical latitudes can survive with any appreciable amplitude by the time they reach equatorial latitudes (Deser et al. 1996; Schneider et al. 1999). An alternative role for the STCs in decadal climate variability is that variations in pycnocline transport act on the mean hydrographic structure and are primarily responsible for changes in equatorial SSTs (Kleeman et al. 1999; Nonaka et al. 2002). This latter hypothesis is supported by observational studies (e.g., McPhaden and Zhang 2002, 2004) and coarse-resolution ocean general circulation model simulations (e.g., Lee and Fukumori 2003; Capotondi et al. 2005).

The strength of the STCs can be represented by the transport in its lower limb, namely, the volume transport of water in the ocean pycnocline layers. In observational studies, ocean subsurface hydrographic data are used to estimate the geostrophic transport beneath the surface layer, but data are not adequate to define decadal variations in western boundary current transports that represent a significant fraction of STC pycnocline transport (Liu 1994). Modeling studies (Lee and Fukumori 2003; Capotondi et al. 2005) also suggest a partial compensation between the interior ocean and western boundary pycnocline transport variability. Yet, the representation of western boundary transport in those models is questionable because of their coarse resolution.

In this study, we investigate variations of the Pacific STC transport for the period 1992–2003 in an eddy-resolving ocean general circulation model. The model was forced with 6-hourly European Centre for Medium-Range Weather Forecasts (ECMWF) reanalysis and operational analysis surface fluxes. Our study has three specific purposes. First, the observational study by McPhaden and Zhang (2004) shows an upward trend in the STC transport in the Pacific from the early 1990s to early 2000s, indicating that this circulation has rebounded from a less active state that has lasted since the 1976/77 regime shift in the Pacific basin. As acknowledged by McPhaden and Zhang (2004), there are considerable uncertainties in their calculations because the observations are sparse in space and time, the geostrophic method requires assumptions about a level of no motion, and decadal variations in western boundary current transport cannot be reliably estimated. A model simulation where all ocean fields are available at high resolution provides a valuable dataset for improving our understanding of the relevant processes.

Second, we seek to understand the relationships between the meridional transport of the STCs in the pycnocline, the Equatorial Undercurrent (EUC), and the upwelling into the mixed layer in the eastern tropi-

cal Pacific. In the context of ventilated thermocline theory (Luyten et al. 1983), all of these transports can be viewed as branches of the STC: water subducted in the subtropical outcrop region eventually joins the EUC after an intricate pathway through the ocean interior and the western boundary (Pedlosky 1987, 1988; Liu et al. 1994). The water is then transported eastward by the EUC, and finally upwells to the surface layers in the eastern basin. However, very few studies have addressed the issue of decadal variations in EUC transports and how they relate to STC variability (Chang et al. 2001). Here we use long time series data from the Tropical Atmosphere–Ocean/Triangle Trans-Ocean Buoy Network (TAO/TRITON) array (McPhaden et al. 1998) to validate model EUC variations and relate EUC transports to other branches of the Pacific STCs.

The third purpose is to examine how the upper-ocean heat balance in the tropical Pacific is influenced by the volume transport variability of STC on decadal time scales. Previous studies (e.g., Hazeleger et al. 2004) have suggested that total poleward heat transport in the tropical ocean is controlled by local wind-driven overturning and gyre circulations, as well as by extratropical buoyancy-flux-driven overturning that reaches into the Tropics. In this study, we will examine the relationship between anomalous pycnocline volume transport, its associated heat transport, and SST using an idealized model. We will also examine the relative contributions of circulation and temperature anomalies to the heat transport. Since modeling assessments of role of ocean circulation on the upper-ocean heat budget depend on model physics, particularly mixing parameterizations, our results will be compared with available modeling studies to indicate model sensitivity.

The paper is organized as follows: In section 2 we introduce the ocean general circulation model and the atmospheric forcing data used in this study. The results in terms of STC volume transports, their decadal variability and relationships to the EUC and equatorial upwelling, and impacts on upper-ocean heat balance in the Tropics are presented in section 3. In section 4 we compare some of our results to other recently published modeling results and discuss this particular model's limitations. We summarize our main conclusions in section 5.

2. Model

The model used in this study is the Hybrid Coordinate Ocean Model (HYCOM) (Bleck 2002; see information online at http://hycom.rsmas.miami.edu). It covers the Pacific Ocean from 20°S to 66°N. Using Merca-

tor projection, the horizontal grid resolution is 0.08° in longitude by $0.08°\cos(\phi)$ in latitude, where ϕ is the latitude. This gives a midlatitude grid spacing of approximately 6 km and a tropical spacing of just under 9 km. It has 20 vertical coordinate surfaces that are typically isopycnal in the open, stratified ocean but makes a dynamically smooth transition to terrain-following coordinates in shallow coastal regions and to z-level coordinates in the mixed layer and/or unstratified waters. The hybrid coordinate is obtained via a fully general continuity equation that allows an arbitrary partitioning between density coordinates and depth coordinates on a time step by time step basis. Specific details about the numerics can be found in Bleck et al. (2002), and additional case studies can be found in Chassignet et al. (2003).

HYCOM is configured with several different mixed layer formulations (see Halliwell 2004, for more details), but the K-profile parameterization (Large et al. 1994) is used exclusively here. The bathymetry is based on a merging of the global 5′ Digital Elevation Model (ETOP05) (National Oceanic and Atmospheric Administration 1986) and Smith and Sandwell (1997) data with numerous hand edits. Closed boundaries are used for the Indonesian Throughflow region and in the Bering Strait. Along the southern boundary, the ocean temperature and salinity are relaxed to 3D monthly climatological data from the Generalized Digital Environmental Model (GDEM), version 3, (Carnes 2002) in a 3°-wide buffer zone. The deformation-dependent Laplacian viscosity factor is 0.1 and a combination of Laplacian (0.005) and biharmonic (0.01) momentum dissipation is used for the large and small scales, respectively.

The model was initialized from a 0.16° version of Pacific HYCOM and spun up at 0.08° to near equilibrium using a climatology of winds and thermal forcing based on the 1979–93 ECMWF Reanalysis atmospheric products. After spin up, the simulation was extended using the 6-hourly 1979–93 ECMWF Reanalysis and then 1994–2003 ECMWF operational forcing. No significant basinwide changes in forcing were detected across the 1993–94 time boundary. The 10-m wind velocity components were converted to stresses using a stability-dependent drag coefficient from Kara et al. (2002). Thermal forcing includes air temperature, specific humidity, and radiative (shortwave and longwave) fluxes. Precipitation is also included as a surface forcing. Surface latent and sensible heat fluxes are calculated using "bulk formulae" given the above atmospheric conditions and model SST. Model sea surface salinity (SSS) is relaxed to monthly GDEM3 SSS, but no SST relaxation is used by HYCOM. Monthly river runoff is parameterized as a
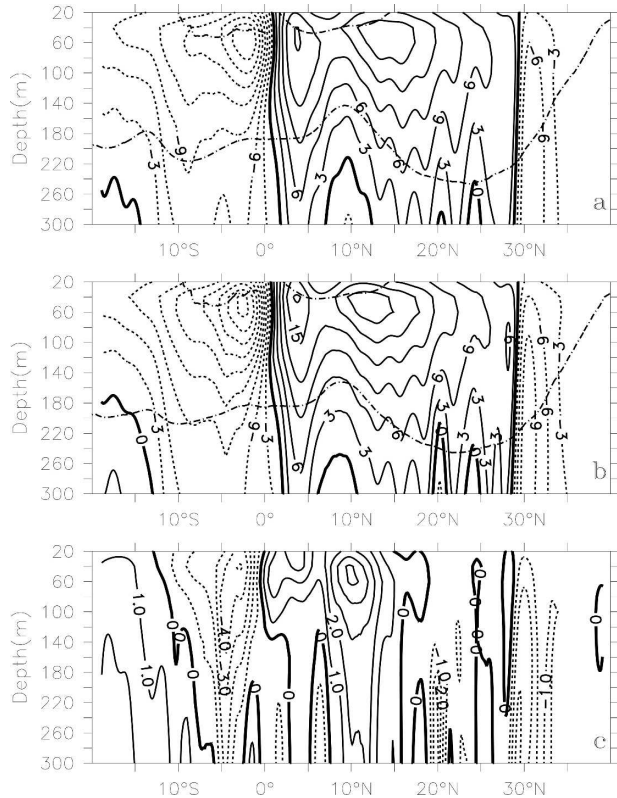

FIG. 1. Meridional overturning circulation in the top 300 m of the model (Sv). Solid (dashed) lines indicate clockwise (counterclockwise) circulations. Dashed–dotted lines indicate the 22.5 and 25.3 σ_θ surfaces. Mean state for (a) Period 1 (defined in the text), (b) Period 2 (defined in the text), and (c) the difference between Periods 1 and 2, (b) minus (a), are shown.

surface precipitation flux at a select number of locations, and oceanic turbidity is also taken into account after the work of Kara et al. (2005).

All model output used in this study consists of monthly averages from year 1992 to 2003. The reason we focus on this period is to facilitate a direct comparison with the observational study of McPhaden and Zhang (2004), which covers roughly the same time frame. This period is long enough for us to detect decadal changes in the system by averaging over two full ENSO cycles (each 5–6 yr long). Choosing this period to study also allows us to compare the model simulation with high accuracy in situ ocean observations, which are available for this most recent decade.

3. Results

a. STC pycnocline transport and its variability

The mean overturning circulation in the model's upper ocean (Fig. 1) is obtained by interpolating meridi-
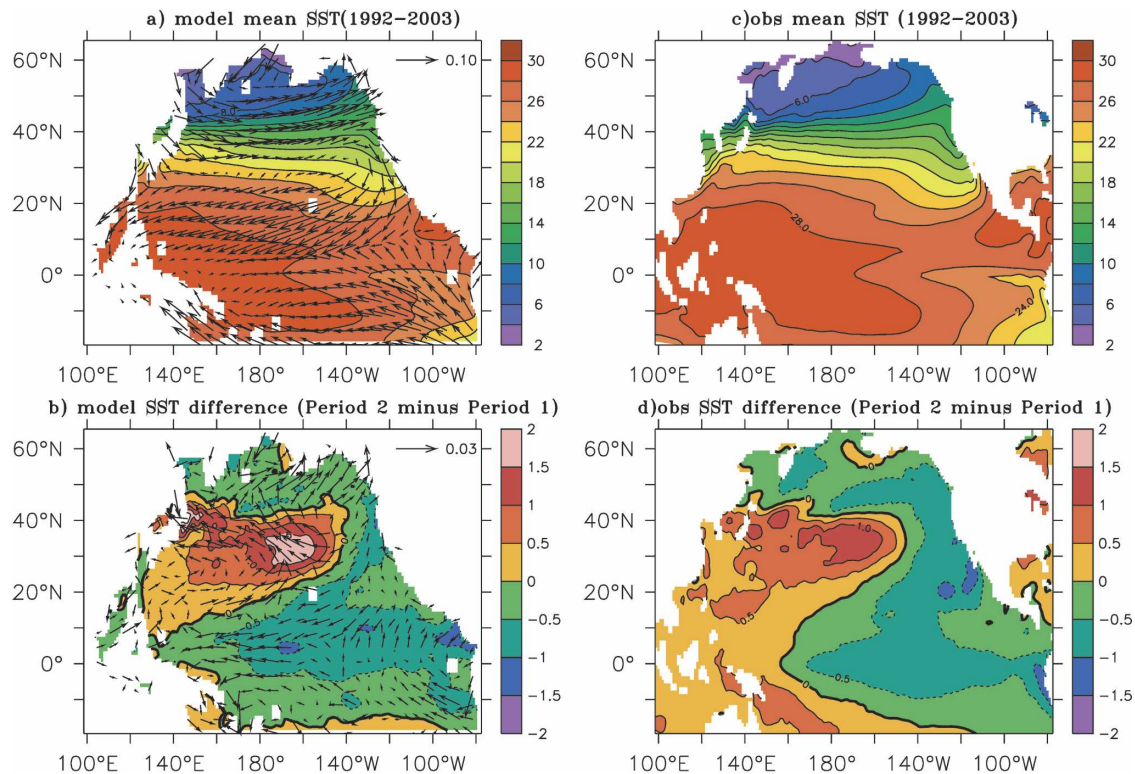
FIG. 2. (a) Modeled mean SST averaged for all months from 1992 to 2003. (b) Modeled SST difference between the two periods (Period 2 minus Period 1). (c) Observed mean SST averaged for all months from 1992 to 2003. (d) Observed SST difference between the two periods (Period 2 minus Period 1). Units are °C. Overplotted is the mean wind stress [in (a)] and the wind stress difference for Period 2 minus Period 1 [in (b)]. Unit of wind stress: N m^{-2}.

onal velocity in HYCOM's hybrid vertical coordinate to fixed depth (the interpolation interval is 20 m) and then integrating zonally and vertically the interpolated meridional velocity. The advantage of this presentation is that it gives a visual impression of where the circulation takes place in latitude and depth: the disadvantage of depth averaging though is that it can create spurious circulation cells in regions of sloping isopycnals (Hazeleger et al. 2001). For example, the so-called tropical cells, which are local circulation within 5° of the equator in both hemispheres, are a known artifact of fixed-depth averaging. Ignoring the tropical cells, circulation associated with subtropical subduction is centered between 50- and 200-m depths. This circulation has intensified by 2–3 Sv (Sv ≡ 10^6 m^3 s^{-1}) in both the northern and southern branch from the time between July 1992 and June 1998 (hereinafter referred to as Period 1) to between July 1998 and June 2003 (hereinafter referred to as Period 2) (Fig. 1c). These two periods were chosen as in McPhaden and Zhang (2004) because each spans one complete ENSO cycle. In addition, the observed Pacific decadal oscillation (PDO) index dropped significantly from Period 1 to Period 2 (see McPhaden and Zhang 2004 for more details).

The simulated mean SST (Fig. 2a) is reasonably close to observations (Fig. 2c). In particular, the eastern equatorial cold tongue is captured in the model, although its amplitude is somewhat weaker than observed. Over most of the Pacific, the absolute values of discrepancies between the simulated and observed SST averaged for the full study period are less than 1°C (not shown). The modeled SST difference between Periods 1 and 2 (Fig. 2b) is characterized by an antiphase relation between the midlatitude North Pacific and tropical Pacific anomalies. During Period 2 when the STC is stronger, positive SST anomalies (relative to those during Period 1) developed in the midlatitude belt between 20° and 40°N, with maximum values situated in the middle of the basin; concomitantly, negative SST anomalies exist in the Tropics and in the nearshore waters off the west coast of North America. The modeled SST anomaly pattern is similar to its observational counterpart (Fig. 2d). Both of these patterns represent the canonical pattern of SST anomalies associated with the PDO (Mantua et al. 1997; Latif and Barnett 1994), although in the model the tropical SST anomaly penetrates farther to the west than in observations.
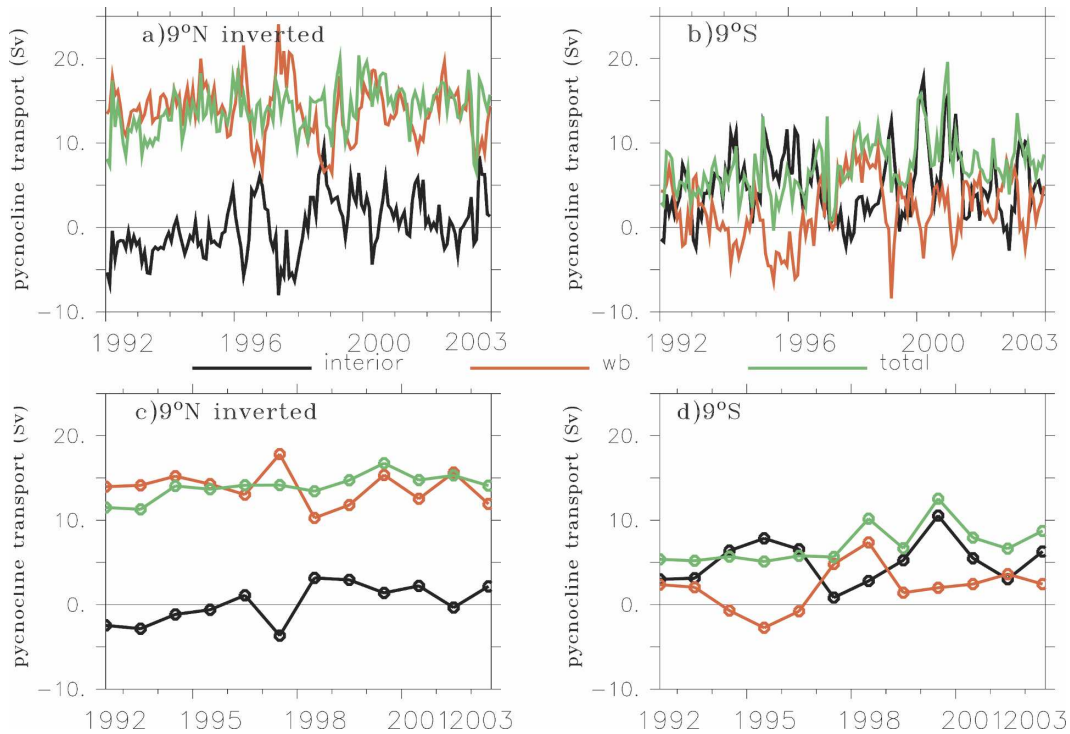
FIG. 3. Pycnocline volume transport at 9°N and 9°S as a function of time. The results at 9°N are inverted for easy comparison. (a), (b) Monthly data and (c), (d) annual averages of the monthly means are shown. Black, red, and green lines represent the interior ocean, western boundary, and total across the basin transport, respectively. The interior ocean and western boundary subdomain is separated by 145°E (160°E) for the transport at 9°N (9°S).

The wind stress anomaly from Period 1 to Period 2 (Fig. 2b) shows an overall strengthening of the trade winds. Stronger trade winds would cause the tropical thermocline to slope down even more to the west. The resulting thermocline tilt anomalies would be consistent with the stronger equatorward flow in the pycnocline shown in Fig. 1c. Notice also that the wind stress anomalies extend to the extratropics and may impact subtropical subduction and therefore tropical thermocline ventilation.

The volume transports in the model's pycnocline across 9°N and 9°S as a function of time are presented in Fig. 3. They are calculated using modeled meridional velocity and layer thickness on the original vertical coordinates without interpolation. The latitude 9°N is chosen because it is a choke point in the communication between the subtropics and Tropics owing to the existence of a potential vorticity (PV) ridge at this latitude (Figs. 4a,b); 9°S is chosen for hemispheric symmetry. Throughout this paper, the model pycnocline is defined as the layers between the 22.5 and 25.3 σ_θ surfaces (red lines in Fig. 1) because it captures the density range over which the majority of equatorward flow takes place in the model. This range of density classes significantly overlaps with, but is slightly lower than,

that analyzed by McPhaden and Zhang (2002, 2004) from observations. The total transport across the basin is divided between the interior ocean (east of 145°E at 9°N and east of 160°E at 9°S) and the western boundary (longitudes west of 145° and 160°E, respectively). The anticorrelation between the components (named as "interior" and "wb" in Fig. 3) suggests that transport anomalies through each region tend to compensate each other on interannual time scales, but there are exceptions. For example, in the annual average transport time series at 9°S (Fig. 3d), the anticorrelation between the western boundary and interior transport deteriorated in the latter part of the record. Moreover, this compensation is only partial such that the trend in the total transport across the basin follows that of the interior ocean transport. This partial compensation is consistent with indirect estimates of western boundary current (WBC) transport (McPhaden and Zhang 2004) and other forced model simulations (Lee and Fukumori 2003; Hazeleger et al. 2004; Capotondi et al. 2005), which showed that the reduction in interior ocean transport convergence from the mid-1970s to earlier 1990s was partially compensated by WBC transports.

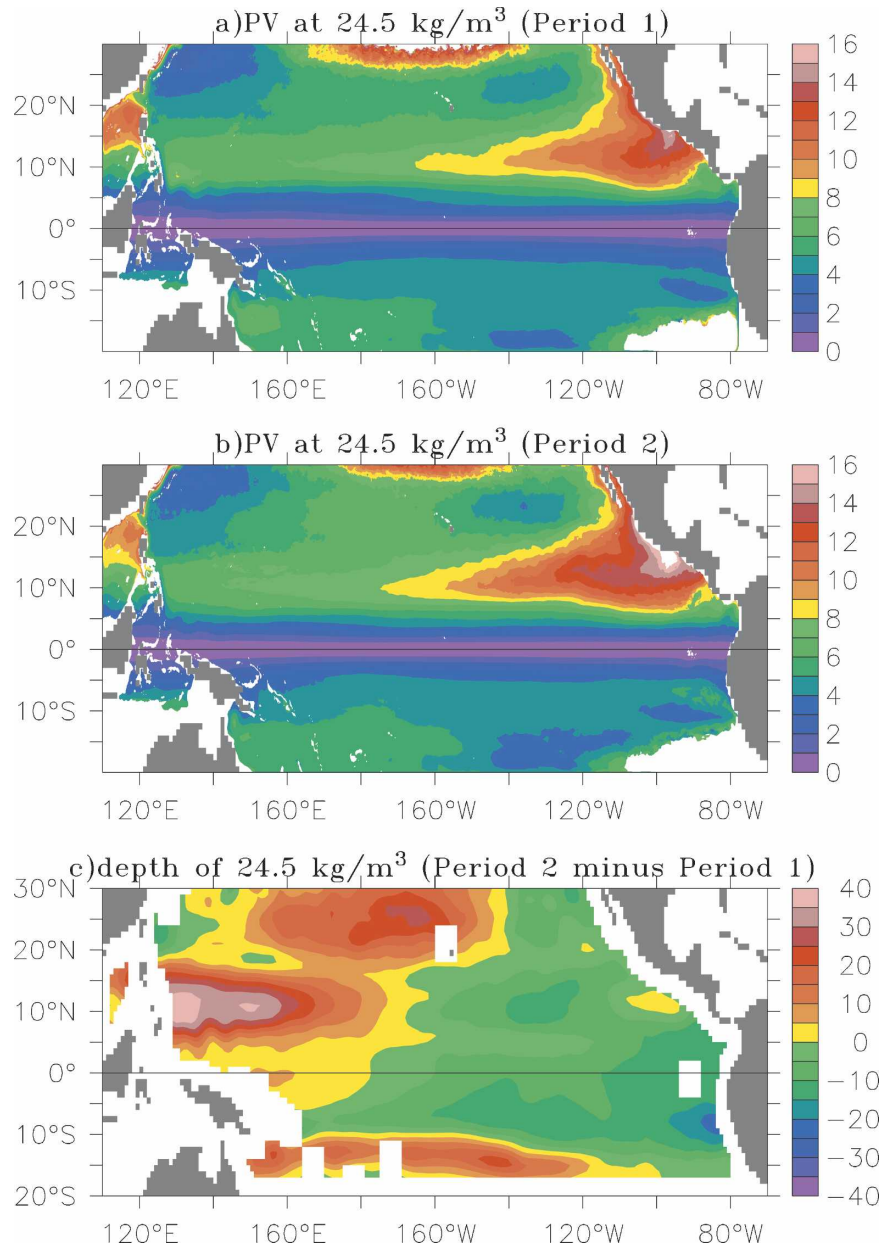The total pycnocline transport convergence across the basin averaged for Periods 1 and 2 is 19.0 ± 0.6 Sv

FIG. 4. Absolute value of potential vorticity (10^{-10} m^{-1} s^{-1}) on the 24.5-σ_θ surface averaged for (a) Period 1 and (b) Period 2. (c) Difference in the mean depth of the 24.5-σ_θ surface for Period 2 minus Period 1.

and 23.9 ± 0.8 Sv, respectively. Standard errors throughout this study are calculated as $\sigma/\sqrt{N}$, where σ is the standard deviation of monthly transport for each period and N is the number of degrees of freedom estimated assuming the transport is an autoregressive process (Davis 1976). Therefore, the total pycnocline transport convergence in the model increased by 4.9 ± 1.0 Sv from Period 1 to Period 2 (Table 1). The primary contribution to this increase comes from interior ocean

transport convergence, which is increased by 4.5 ± 1.6 Sv from 3.4 ± 1.2 Sv in Period 1 to 7.9 ± 1.1 Sv in Period 2 (Table 1). These modeled interior ocean mean transport values are significantly lower than the geostrophic estimates of 13.4 ± 1.6 Sv in Period 1 and 24.1 ± 1.8 Sv in Period 2 found in McPhaden and Zhang (2004). There are several possible reasons for this model–observation discrepancy, which will be discussed later. However, most important for our pur-

TABLE 1. Mean transport of various branches of the STC and the standard errors estimated from monthly data. Pycnocline transports include the transport convergences at 9°N and 9°S for the interior ocean and total across-basin components. EUC transport is defined at 140°W. The upwelling is integrated over the region 9°N–9°S, 90°W–180°. We estimated the standard errors of the difference between the means as $\sqrt{e_1^2 + e_2^2}$, where e_1 and e_2 is the standard error for each period.

Branch	Period 1	Period 2	Period 2 − Period 1
Total pycnocline transport	19.0 ± 0.6 Sv	23.9 ± 0.8 Sv	4.9 ± 1.0 Sv
Interior pycnocline transport	3.4 ± 1.2 Sv	7.9 ± 1.1 Sv	4.5 ± 1.6 Sv
EUC	27.2 ± 2.1 Sv	33.1 ± 2.2 Sv	5.9 ± 3.0 Sv
Upwelling	11.7 ± 2.1 Sv	16.6 ± 4.0 Sv	4.9 ± 4.5 Sv

poses, there is a significant increase in interior ocean pycnocline volume transport from Period 1 to Period 2, in qualitative agreement with the observations.

As mentioned earlier, the spatial pattern of the SST anomaly suggests that, when the STCs are stronger (weaker), tropical SSTs are cooler (warmer) (Fig. 2b). This relationship is further investigated in the temporal domain (Fig. 5). The simultaneous correlation coefficient between monthly interior ocean pycnocline transport convergence across 9°N and 9°S and SST anomaly averaged in the eastern tropical Pacific (9°N–9°S, 180°–90°W) is −0.7 (statistically significant at a 95% confidence level). Lagged cross-correlation function (not shown) indicates that the maximum correlation occurs

when the former leads the latter by 2 months. The correlation coefficient decreases to 0.4 when the total transport across the entire latitude circle is used in the calculation, which is still statistically significant but only marginally. This decrease in correlation is expected given the partial compensation of the western boundary transport anomalies and interior ocean transport variations.

The zonal structure of STC pycnocline transport can be seen in the accumulated integration of the transport westward from the eastern boundary (Fig. 6). We have done this calculation for the 9°N and 9°S sections, as well as for the 13°N and 13°S sections, to investigate if there are meridional variations in the zonal structure, and also because other models have shown that transport variations at 13°N and 13°S are larger than at 9°N and 9°S (Capotondi et al. 2005). For the Northern Hemisphere branch, most of the equatorward flow occurs between 140°E and 180°, while for the Southern Hemisphere branch, the equatorward transport starts farther east at 140°W. These zonal structures are similar qualitatively for the two latitudes within each hemisphere, but the mean equatorward transport as well as the transport difference between Periods 1 and 2 are in general larger at the higher latitudes.

Differences in the zonal structure between the Northern and Southern Hemispheres are caused by the existence of a potential vorticity ridge in the Northern Hemisphere but not in the Southern Hemisphere (Fig. 4). Following McPhaden and Zhang (2004), potential vorticity is defined as $\rho_o^{-1} f dp/dz$, where f is the Coriolis
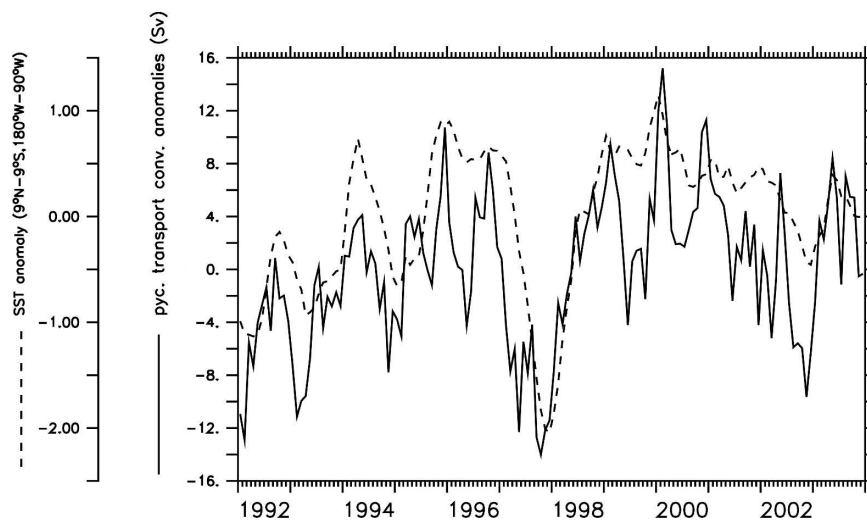

FIG. 5. Solid line: Time series of the interior ocean pycnocline transport convergence across 9°N and 9°S. Shown are monthly anomalies relative to the climatological annual cycle. Dashed line: time series of monthly SST anomaly (°C) averaged in the eastern tropical Pacific from 9°S to 9°N, 180° to 90°W. The SST time series is inverted for easy comparison.
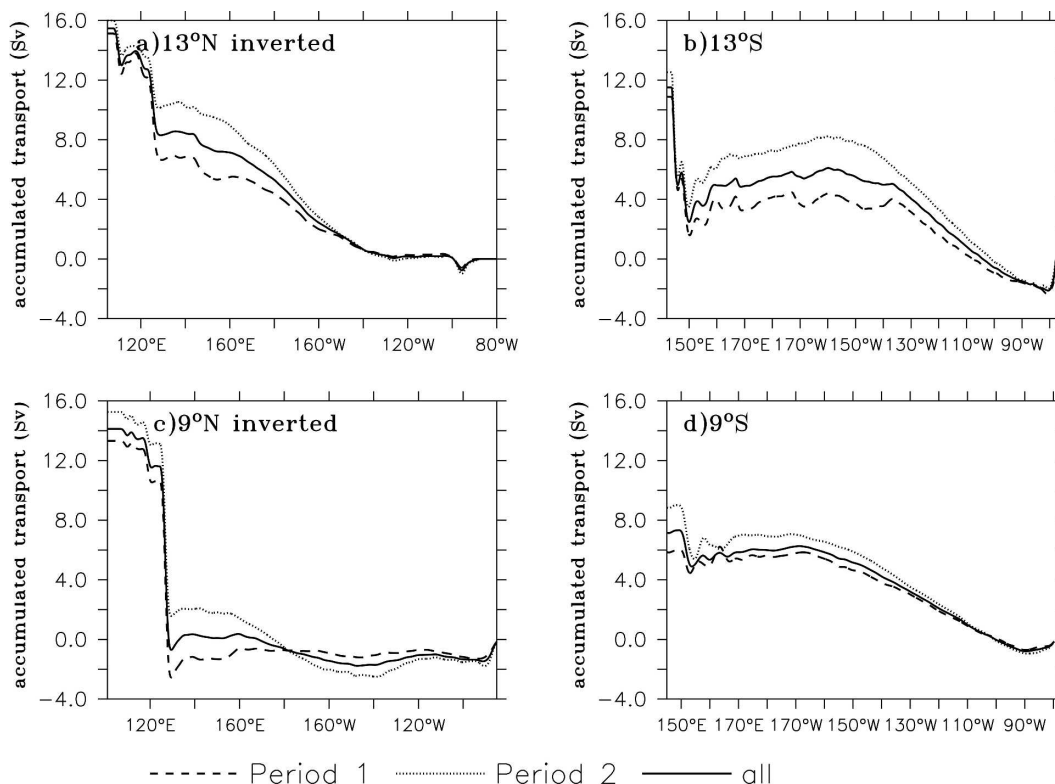
FIG. 6. Zonally accumulated pycnocline transport as a function of longitude. The integration is started from the eastern boundary and accumulates westward. The latitude at which the computation is performed is marked on the plots. Dashed lines represent averages for Period 1, dotted lines for Period 2, and solid lines for all 12 years of data.

parameter, dp/dz is the vertical density gradient, and ρ_o, is a constant reference density (10^3 kg m^{-3}). We calculate PV on the 24.5-σ_θ surface, which is situated vertically at the center of the model pycnocline. The spatial structure of the simulated PV field is remarkably close to that shown in McPhaden and Zhang (2004, their Fig. 2), although quantitative differences still exist. The spatial pattern indicates that under the influence of the intertropical convergence zone (ITCZ), a high PV ridge extends from the Central American coast to about 160°W in the northern subtropics. Therefore water subducted in the northern subtropics has to move westward parallel to PV contours (assuming PV is conserved) before turning southward in the central basin, causing weak equatorward flows in the eastern basin. In contrast, water in the Southern Hemisphere can move equatorward even in the eastern basin because of the lack of PV ridge there.

The difference in the mean depth of the $\sigma_\theta = 24.5$ surface between the two periods (Fig. 4c) shows that the zonal slope of this isopycnal surface increases with time, owing to shoaling in the eastern basin and deepening in the western basin at 9°N, and primarily to shoaling in the eastern basin at 9°S. This increase in

isopycnal slope is consistent with changes in surface wind stress (Fig. 2b) and the upward trend in the pycnocline transport (Fig. 3).

The separation of the lines representing averages for Periods 1 and 2 in the interior basin and the tendency for them to merge in the western boundary (Fig. 6) again demonstrates the partial compensation between interior and western boundary transports, but the degree of compensation is both temporally and spatially varying. For example, compensation is not obvious for 9°S (Fig. 6d), where the difference in the mean transports for the two periods in the interior ocean remains in the western boundary. Judging from the transport time series (Fig. 3d), the breakdown of the anticorrelation between the interior and western boundary transport anomalies only occurred in the later period. Lee and Fukumori (2003) argue that the compensation is caused by the fact that the pycnocline transport is controlled by both the overturning circulation and the horizontal gyre circulation, while Capotondi et al. (2005) suggest that it can be caused by westward propagation of Rossby waves as the ocean dynamically adjusts to surface wind forcing changes. Whatever the mechanism, our results using an eddy-resolving model in gen-
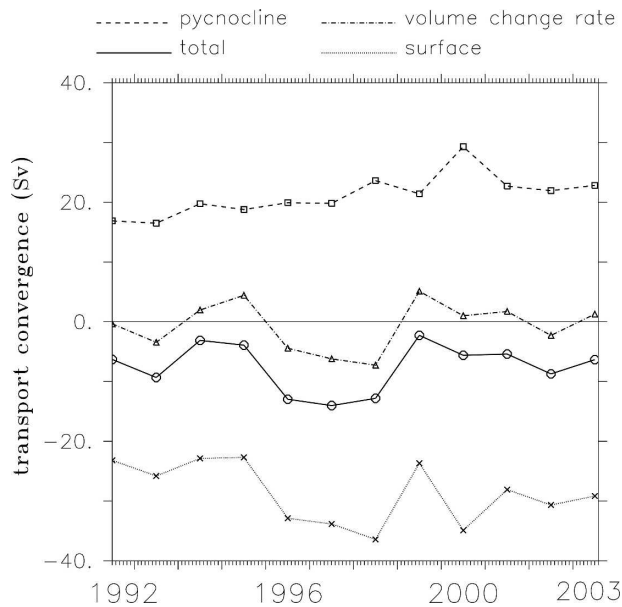
FIG. 7. Mass budget of the tropical control volume defined as the region from the surface to the 25.3-σ_θ isopycnal in the vertical and 9°N to 9°S latitudinally across the entire basin. Shown are annually averaged data: "surface," "pycnocline," and "total" in the legend refers to meridional transport convergence across the basin through the surface layers, the pycnocline layers, and all layers, respectively, of the control volume.

eral corroborate these earlier coarse-resolution model results about the importance of western boundary current compensation on decadal time scales.

b. Influence of STC on the mass balance of the tropical ocean

To examine the mass balance, we define a control volume as the region from the surface to the 25.3-σ_θ isopycnal in the vertical and from 9°S to 9°N latitudinally across the entire basin. The total transport convergence across the northern and southern boundaries of this box is the summation of the pycnocline transport convergence and the surface transport divergence (Fig. 7). As in the above subsection, the pycnocline transport is calculated using model meridional velocity and layer thickness across the basin between 22.5 and 25.3 σ_θ surfaces excluding the mixed layer when the 22.5-σ_θ surface outcrops. The surface transport divergence is calculated from the surface to the 22.5-σ_θ surface, or to the base of the mixed layer (defined as the depth at which temperature is 0.2°C colder than SST) when the 22.5 σ_θ outcrops. For clarity, we only show annual mean data in Fig. 7, but the conclusion remains the same when monthly data is used. Both pycnocline convergence and surface divergence show a decadal trend toward increasing values with time. These in-

creases nearly compensate each other, causing the total meridional transport convergence across the lateral boundaries of the control volume (black line in Fig. 7) to be quasi steady and much smaller in magnitude than either component. As has been observed in previous modeling studies of El Niño and La Niña (e.g., Springer et al. 1990), there is also a tendency for compensation between the pycnocline transport convergence and surface transport divergence on interannual time scales, especially between 1997 and 2000.

Total meridional transport convergence into the control volume is negative, and there is a near-constant offset between this convergence and the time rate of change of the control volume. This offset implies a steady upwelling through the base of 25.3-σ_θ surface between 9°S and 9°N. However, because this upwelling is located at the base of the pycnocline, it does not represent a contribution of STCs to equatorial upwelling.

c. EUC, equatorial upwelling, and their relationships to STC meridional transport

In this section we examine variations in EUC transport and equatorial upwelling relative to other branches of the STCs. As a first step, we validate the model EUC against observations. The meridional and vertical structure of the zonal flow in the model (Fig. 8a) is very similar to shipboard observations (Johnson et al. 2001, their Fig. 2a). At 136°W, the core of EUC is located at 0°, 120 m in the simulation (compared to 0°, 110 m in observation), and its maximum velocity reaches 90 cm s^{-1}, the same as in observations. Results from year 1999 are shown here as an example, but comparisons for other years are equally good. The simulation also captures other observed current structures in the tropical ocean: the northern branch of the South Equatorial Current (SEC) with a surface core at 2°N, the southern branch of SEC with a surface core at 4°S, and the North Equatorial Countercurrent (NECC) with its core centered at 50 m along 7°N. Although not particularly obvious in Fig. 8a, two subsurface countercurrents also exist in the simulation, at least for some years. In the zonal direction, the modeled EUC axis along the equator tilts upward from west to east (Fig. 8b), with the maximum velocities situated between 155° and 120°W. Both tilt and zonal structure are consistent with observations (Johnson et al. 2001, their Fig. 3a).

The zonal flow at the equator has been monitored continuously by ADCP measurements from the early 1990s to the present (Plimpton et al. 2004), providing an opportunity for us to compare these data with the simulation. At 140°W, vertically integrated zonal flow in the
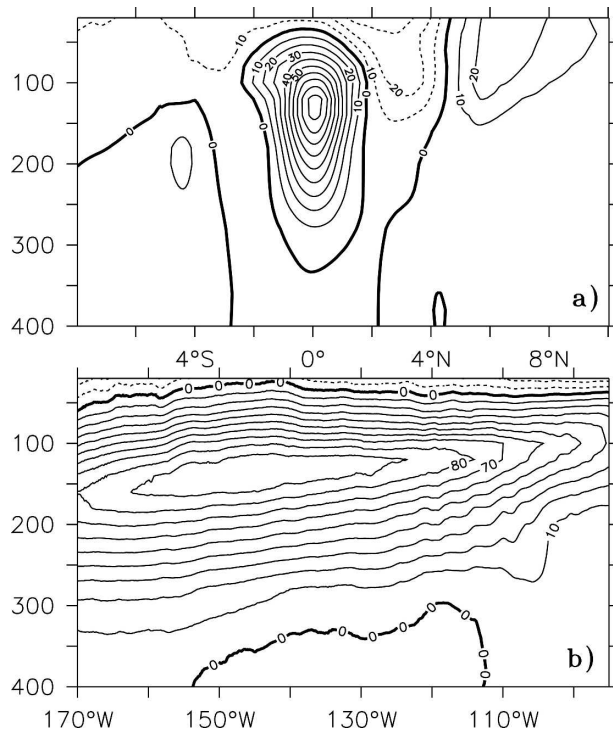
FIG. 8. Annual mean zonal velocity field in the model. Results are shown for year 1999: (a) Meridional section at 136°W from 8°S to 10°N; (b) zonal section at the equator from 170° to 95°W. Contour interval is 10 cm s^{-1} in both plots. Positive values indicate eastward flow.

FIG. 9. (a) Zonal flow at the equator integrated from the shallowest data point to 400-m depth (units: m^2 s^{-1}), solid line from ADCP data and dashed from the HYCOM simulation. The shallowest (deepest) ADCP data at this longitude are at 10-m (415-m) depth. (b) Scatterplot of modeled zonal flow at the equator vs the modeled EUC transport (Sv). Zonal flow integrated both vertically and meridionally (from 2°S to 2°N). The vertical integration in both cases is from the shallowest model layer to 400-m depth. (c) EUC transport time series from the model: Horizontal lines denote the mean transport for Period 1 and Period 2, respectively. All data shown are at 140°W.

model bears a striking resemblance to the ADCP measurements in both amplitude and temporal evolution (Fig. 9a). Comparisons at other longitudes where long records of ADCP data are available (110°W, 170°W, 165°E) indicate that this good comparison is robust across all longitudes. We then computed EUC transport in the model as the integration of zonal velocity with magnitude larger than 10 cm s^{-1} from the shallowest model layer to 400-m depth and from 2°S to 2°N. These transport estimates are highly correlated with estimates of the vertically integrated zonal flow at the equator (Fig. 9b), as in observations (e.g., Knox and Halpern 1982). Based on Figs. 9a and 9b, we conclude that EUC transports in the model during this period are very close to observations. The modeled EUC mean transport increased from 27.2 ± 2.1 Sv in Period 1 to 33.1 ± 2.2 Sv in Period 2 (Fig. 9c). The derived difference in the EUC transport (5.9 ± 3.0 Sv) is consistent with the increase in the pycnocline transport convergence across the basin from Period 1 to Period 2, as well as the transport convergence increase in the interior ocean (see discussion in section 3a and Table 1).

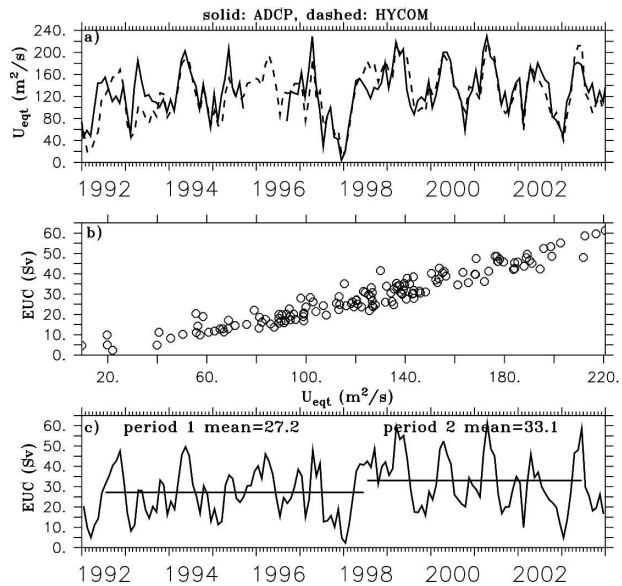Now we compare STC pycnocline transport convergence in the interior ocean with upwelling in the east-ern tropical Pacific. Using the total across-basin transport did not change the basic conclusion although it lowered the correlation coefficient (see details below). Here the upwelling transport is calculated as the spatially integrated vertical velocity at the base of the mixed layer. The spatial domain is chosen to be 9°N–9°S, 180°–90°W [the same index region for SST variability in McPhaden and Zhang (2004) and Fig. 4 herein]. The resulting upwelling transport is highly correlated with the pycnocline transport convergence with no obvious lag (Fig. 10). The simultaneous correlation coefficient between the monthly time series (Fig. 10a) is 0.76 (statistically significant at a 95% confidence level, lowered to 0.64 when cross-basin pycnocline transport convergence was used). The averaged upwelling transports for Periods 1 and 2 are 11.7 ± 2.1 Sv and 16.6 ± 4.0 Sv, respectively. These values correspond well with the 1993–99 mean cross-isothermal upwelling transport near the base of the surface mixed layer of 15 Sv computed from observed winds and upper-ocean thermal field between 5°N and 5°S, 95° and 155°W (Meinen et al. 2001).

The interrelationship between pycnocline transport in the interior ocean, EUC, and eastern basin upwelling
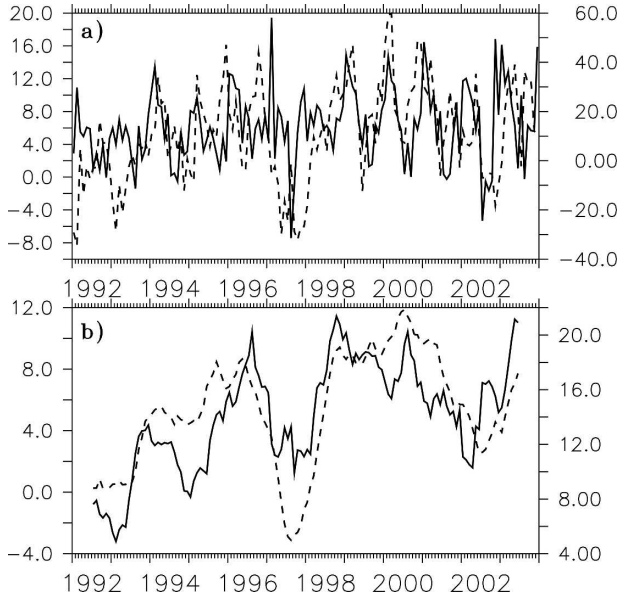
FIG. 10. (a) Relationship between the interior-ocean pycnocline transport convergence across 9°N and 9°S (solid line, using the left coordinate; units: Sv) and the upwelling at the base of mixed layer spatially integrated over 9°N–9°S, 180°–90°W (dashed line, using the right coordinate; units: Sv). (b) As in (a), except now the monthly data were filtered by a 13-point running mean filter.

is summarized in Fig. 11. These time series are highly cross correlated at zero lag. The correlation coefficient between the filtered pycnocline transport convergence and EUC transport (upwelling) is 0.7 (0.6), which is statistically significant with a 95% confidence level.

The absolute mean transport amplitudes of these variables, in addition to those of the total transport convergence across the basin for Periods 1 and 2, and the differences between the two periods, are listed in Table 1. Bearing in mind the uncertainties represented by the standard errors in each transport estimate, these values indicate that the increase in upwelling between the two periods (4.9 ± 4.5 Sv) is dynamically consistent with the increases in both equatorward pycnocline transport and EUC transport; furthermore, the increase in the across-basin pycnocline transport convergence is dominated by that in the interior ocean.

d. Impacts on meridional heat transport

To understand the impact of STC variations on the upper-ocean heat balance, we calculated meridional heat transport associated with STC as

$$H(y, t) = \sum_{z=\text{pyc}} \int (VhT)|_{x,y,z,t} \, dx$$
$$- T_{\text{Ek}}(y, t) \sum_{z=\text{pyc}} \int (Vh)|_{x,y,z,t} \, dx, \quad (1)$$
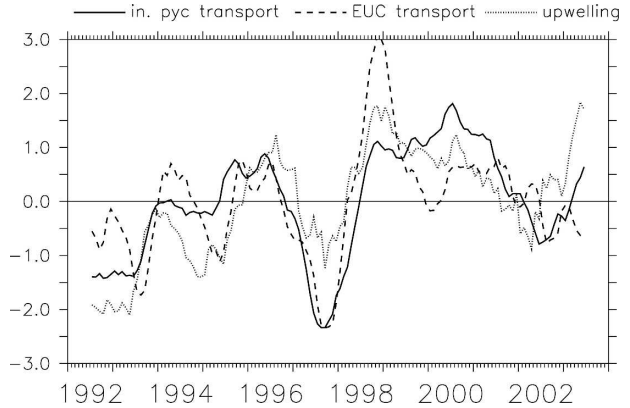

FIG. 11. Comparison between interior-ocean pycnocline transport convergence (black), EUC transport (solid line), and the eastern basin upwelling magnitude (dotted line). For each variable, a monthly climatology based on all 12 years of data for each variable was removed; the resulting monthly anomaly time series was then subjected to a 13-point running mean filter. Last, the filtered data were normalized by their respective standard deviations. The corresponding standard deviation for the pycnocline transport convergence, EUC transport, and upwelling magnitude is 3.8, 6.4, and 4.1 Sv, respectively.

where $\Sigma_{z=\text{pyc}} \int dx$ denotes zonal integration across the basin and then vertical summation over the range of the pycnocline, and v, h, and T are layer meridional velocity, thickness, and temperature, respectively. Here H can be scaled to PW by multiplying with $\rho C_p \times 10^{-15}$, where $\rho = 1026$ kg m^{-3} and $C_p = 3990$ J K^{-1} kg^{-1}.

Equation (1) represents an idealized model of heat transport by the STCs in which we assume that the upper branch of the STC in the Ekman layer carries the same amount of transport as in the pycnocline layer with a zonal mean temperature of $T_{\text{Ek}}(y, t)$. In practice, $T_{\text{Ek}}(y, t)$ is calculated as the volume-weighted zonal-mean mixed layer temperature. The advantage of this formula is that it ensures a mass balance so that we can define a "heat transport" associated with the STCs as a function of time. Errors introduced by using this formula will be discussed later.

Thus defined, the long-term mean heat transport divergence of H (computed by subtracting heat transport at 9°S from that at 9°N) is 0.67 ± 0.04 PW, in good agreement with the heat transport divergence associated with the overturning circulation using another idealized model and National Centers for Environmental Prediction (NCEP) surface wind data (Hazeleger et al. 2004).

Because vh and T can be written as $vh = \overline{(vh)} + (vh)'$ and $T = \overline{T} + T'$, where $\overline{(\ )}$ represents long-term time averages and a prime represents deviations from the long-term means, the total heat transport H can be decomposed as
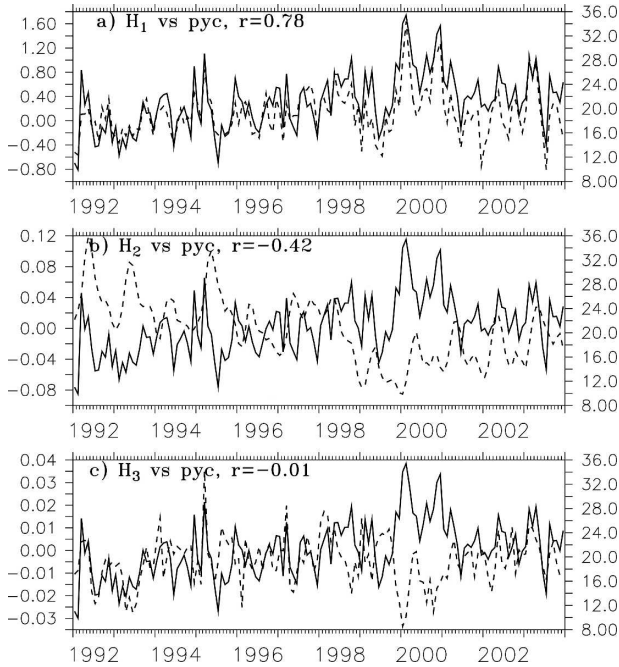
FIG. 12. Relationship between pycnocline volume transport convergence across 9°N and 9°S (solid lines, units: Sv, using the right y axis) and heat transport divergence across the same latitudes (dashed lines lines, units: PW, using the left y axis, negative means convergence). Heat transport divergence is decomposed into contributions from anomalous circulation and thermal anomalies (named as H1, H2, and H3) according to Eqs. (2)–(4) in the text. The correlation coefficient between the two time series in each panel is marked.

$$H = H_m(\overline{vh}, \overline{T}, \overline{T_{Ek}}) + H_1(vh', \overline{T}, \overline{T_{Ek}})$$
$$+ H_2(\overline{vh}, T', T'_{Ek}) + H_3(vh', T', T'_{Ek}), \quad (2)$$

where H_m represents the time-invariant part of H, H_1 represents the effect of circulation anomalies advecting the mean thermal field, H_2 represents the effect of mean circulation advecting thermal anomalies, and H_3 represents the effect of circulation anomalies advecting thermal anomalies.

The divergence of H_1, H_2, and H_3 across 9°N and 9°S and its relationship to pycnocline transport convergence across the same latitudes is shown in Fig. 12. The scale of the left-hand y axis in Fig. 12a is approximately one order of magnitude larger than that in Fig. 12b. Hence, variability of the total heat transport divergence is predominantly controlled by H_1, which, not surprisingly, is highly correlated with pycnocline transport convergence anomalies at zero lag ($r = 0.77$, which is statistically significant at 95% confidence level). In other words, volume transport variability explains about 60% ($r^2 = 0.59$) of the variance in heat transport. Interestingly, H_2 is anticorrelated with pycnocline
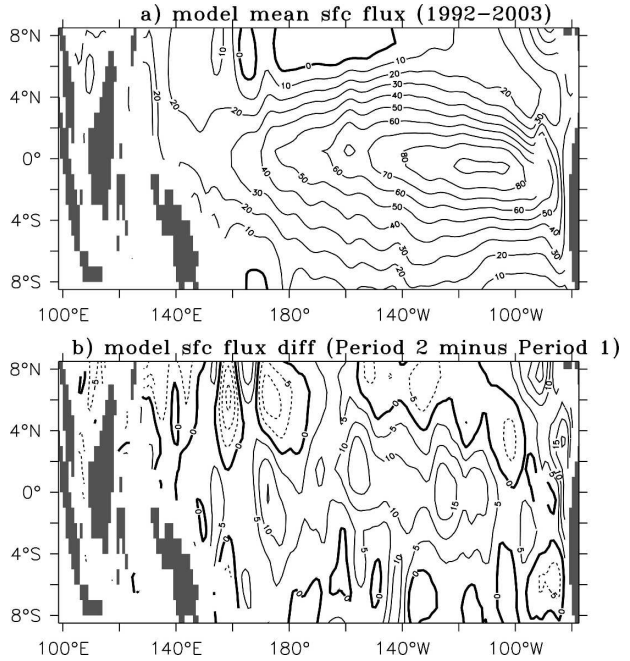

FIG. 13. Net surface heat flux (W m^{-2}), positive means into the ocean, (a) averaged between 1992 and 2003, and (b) the difference Period 1 minus Period 2. Contour interval is 10 (5) for (a) [(b)].

transport convergence anomalies ($r = -0.42$, which is marginally significant at 95% confidence level). The negative correlation can be explained by the interaction of ocean circulation and property fields: as the circulation intensifies from Period 1 to Period 2, tropical upper-ocean temperature decreases, causing the heat transport divergence associated with the thermal anomalies to decrease; hence, a downward trend of H_2 is seen in Fig. 12b. The magnitude of the eddy component H_3 is even smaller than H_2.

The notion that the upper-ocean thermal balance is perturbed by lateral heat transport convergence/divergence is supported by concomitant changes in the net surface heat flux (Fig. 13). From Period 1 to Period 2, net surface heat flux into the ocean between 9°S and 9°N has increased by 0.08 ± 0.05 PW (equivalent to 2.3 ± 1.4 W m^{-1}°C^{-1}), while the H_1 heat transport divergence across 9°S and 9°N has increased by 0.13 ± 0.04 PW. The cooling of the upper ocean from Period 1 to Period 2 is therefore caused by the dominance of anomalous lateral heat transport divergence (a cooling effect) over net surface heat flux anomalies (a heating effect). Using observations and different OGCM simulations, Liu and Huang (2000) attributed the 1945–93 SST warming trend in the tropical Pacific to ocean advection. In their case, tropical SST increases while net surface heat flux has a cooling trend of roughly

10 W m^{-2} (50 yr)$^{-1}$. Both the negative feedback between SST and net surface heat flux and the trend of net surface heat flux [2.3 ± 1.4 W m^{-2} (12 yr)$^{-1}$ in our study versus 10 W m^{-2} (50 yr)$^{-1}$ in Liu and Huang (2000)] are consistent between the two studies.

The 0.13 PW increase in the heat transport divergence of H_1 is 20% of the long-term mean of the total heat transport divergence associated with STC, which is 0.67 PW. It is also comparable to the anomalous heat transport divergence caused by extratropical wind anomalies in an OGCM coupled to a mixed-layer atmospheric model and to El Niño–induced anomalous overturning heat transport divergence in that same model (Hazeleger et al. 2004). In other words, this magnitude of change in the tropical ocean heat transport divergence seems robust across different models.

The main sources of error in the idealized formula of Eq. (1) include the use of zonal mean temperature for calculating temperature transport in the Ekman layer. Also, in our model the contribution of thermal anomalies to the heat transport variations is likely underestimated because spiciness anomalies associated with surface freshwater forcing are suppressed. Because of these errors, the exact values of H and its components should be viewed with caution, but the trends are robust and can be explained by the underlying physics. As the STC increases, the associated poleward heat transport increases, causing the heat transport out of the Tropics to increase; hence the cooling of the tropical upper ocean occurred despite increasing net surface heat flux into the ocean at the same time. As the tropical ocean cools, the poleward heat transport associated with temperature anomalies decreases, but the overall cooling is determined by the intensifying circulation. The result that circulation anomalies dominate over temperature anomalies in bringing about poleward heat transport variations is also found in a 1000-yr integration of a global coupled model (Merryfield and Boer 2005).

4. Discussion

a. Pycnocline transport and extratropical processes

Since pycnocline transport in our calculations is defined at relatively low latitudes (9°N and 9°S), it is possible that this transport and its variations are only driven by tropical winds. However, we cannot rule out the involvement of higher latitudes based on a two-dimensional Eulerian description of the circulation. To examine how the simulated pycnocline transport in the Tropics is related to extratropical subduction, we calculated the subduction rate as the horizontally integrated vertical velocity at the base of the seasonal ther-

mocline defined by the maximum winter mixed layer depth. We neglected contributions from lateral induction, which were found to be small for this region (Huang and Qiu 1994, 1998). The winter (January–March for the North Pacific and June–August for the South Pacific) subduction rate averaged over the 12-yr studying period is approximately 8.5 Sv (or 37 m yr^{-1}) in the South Pacific between 10° and 20°S, 160° and 100°W and 11.8 Sv (or 45 m yr^{-1}) in the North Pacific between 10° and 35°N, 170° and 140°W. The difference of the subduction rate between Periods 1 and 2 (Period 2 minus Period 1) is 3.0 Sv and 0.9 Sv for the North and South Pacific, respectively. These numbers are consistent with the modeled pycnocline transport variations shown in Table 1. With the approximation used in our calculation, they are also broadly consistent with observations.

To ultimately demonstrate the influence of extratropical processes on the tropical ocean circulation, one needs to use Lagrangian methods. Using a passive tracer simulation, Fukumori et al. (2004) showed that roughly 70% of the water mass of the Niño-3 region can be traced back to eastern subtropical thermocline waters on decadal time scales; furthermore, eddy transport due to intraannual variability significantly enhances the transport magnitude of the interior ocean pathways. Passive tracer simulations are beyond the scope of this study, but they would be crucial for understanding the three-dimensional pathways connecting the extratropical and tropical ocean circulations.

b. Relationship between pycnocline transport and SST

A study by Capotondi et al. (2005) using the National Center for Atmospheric Research (NCAR) OGCM suggests that SST anomalies in the equatorial upwelling region lead the STC transport convergence anomaly across 9°N and 9°S by 2 months at maximum correlation (their Fig. 14), whereas in this model SST anomalies lag the STC transport convergence anomalies by 2 months (Fig. 14). In both models the correlation remains statistically significant all the way across the basin interior, indicating that pycnocline transport changes are relevant for SST changes in those regions. The difference in sign of the corresponding phase relationship between the two models needs to be studied further because the role of STC transport in regulating tropical SST depends on the relative timing of each process. Capotondi et al. attributed the time lag of pycnocline transport relative to SST anomalies in the NCAR model to zonal averaging of transport values. Because the STC transport adjusts from the east to the west via oceanic Rossby waves, zonal averaging across
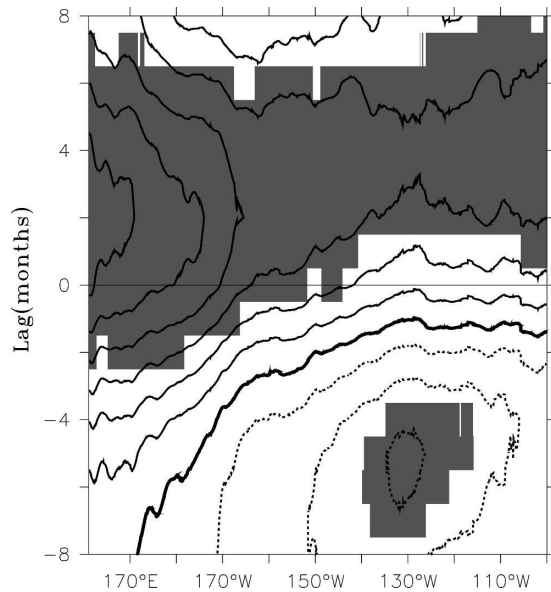
FIG. 14. Cross-correlation between zonally accumulated (starting at 100°W and ending at 160°E) interior-ocean pycnocline transport convergence anomalies across 9°S and 9°N and SST anomalies averaged for 9°N–9°S, 180°–90°W. Positive (negative) lags mean SST anomaly lags (leads) the transport convergence anomaly. Shaded areas indicate that the correlations are statistically significant at a 95% confidence level with the number of degrees of freedom estimated assuming autoregression process (Davis 1976). Dashed (solid) lines indicate negative (positive) correlation. Contour interval is 0.1.

the basin can make the STC transport appear to lag the SST anomaly, which is averaged over the central and eastern Pacific.

We repeated the lagged correlation between the zonally accumulated pycnocline transport and eastern equatorial SST anomaly as in Capotondi et al. (2005) using our model data. The tendency of the maximum correlation to shift in the direction of greater SST lead relative to the pycnocline transport variation as one moves westward is also present in our model (Fig. 14) between 170° and 130°W, but in the western basin (west of 170°W) this effect is not as obvious as that in the NCAR OGCM. The overall smaller zonal slope of the maximum correlation axis in this model compared to that in the NCAR OGCM reflects the model dependence of this result. One possible reason for such model sensitivity is that the baroclinic Rossby wave speed is different between the two models. Although a detailed comparison of baroclinic Rossby wave speed between the models is beyond the scope of this study, we speculate that the HYCOM baroclinic wave speed is generally larger (because its across-basin adjustment time is quicker than the NCAR model according to Fig. 14) owing to its smaller vertical diffusivity in the pycnocline

and stronger stratification. Such model sensitivities need to be kept in mind when interpreting results of model simulations.

Nevertheless, both model simulations show that, when only transport in the eastern part of the basin is considered, the pynocline transport convergence variation leads the SST changes by a few months. There are two possible explanations for this: 1) eastern tropical SST is in part responding to perturbations associated with pycnocline transport anomalies; 2) both eastern tropical SST and pycnocline transport are responding to the same forcing, such as surface wind anomalies, but the pycnocline transport responds quicker than SST. The exact reason(s) for this lead–lag relationship are still not precisely understood, but our results indicate a close relationship between SST and transport variations on interannual to decadal time scales.

c. Model limitations

The model outputs analyzed in this study are monthly averages, so the effects of submonthly time scale variability is not accounted for. High frequency variability may induce additional mass transport variations due to correlations between velocity and isopycnal layer thickness on time scales shorter than 1 month. However, for the domain studied here, the biggest eddy effects are restricted to the equatorial band within 5° of the equator (Hazeleger et al. 2001). Therefore, we do not expect our results to be significantly different when submonthly scale eddy effects are included.

We also have to keep in mind the limited model geometry. Giese et al. (2002) found a strong influence of South Hemisphere processes on the tropical and North Pacific thermocline temperature anomalies. Our model uses a buffer zone at the southern boundary to simulate the South Pacific inflow to the domain. Although it has been suggested that the overturning circulation is relatively insensitive to the buffer layer setup at the lateral boundaries in an isopycnal model (e.g., Smith et al. 2000), the variability of pycnocline transport across the southern boundary in our model is likely underestimated, as reflected in the smaller than observed geostrophic transport differences between Periods 1 and 2 (section 3a). Also, the Indonesian Throughflow (ITF) passage is closed in the model. However, correspondence of our results with those of Lee and Fukumori's (2003) suggests that our basic conclusions may be insensitive to whether the ITF is present or not. Nevertheless, Hazeleger et al. (2004) found that the ITF is important for the heat transport compensation between the overturning circulation and gyre circulation in their model; more specifically, when the ITF is reduced, poleward heat transport in the South Pacific weakens.

The precise role of the ITF in balancing the mean mass and heat transport between different basins on decadal time scales needs to be further clarified.

In addition to model geometry, potential biases in model physics could affect the comparison with observations as well. For example, McCreary and Lu (1994) and Lu et al. (1998) found that the PV ridge in a layer model tends to be too strong and causes an interior ocean equatorward flow that is too weak. In addition, differences can arise because of the sensitivity of models to the specification of mixing parameterizations. Uncertainties in ocean properties specified at lateral open boundaries and in surface forcing variables and computational errors all may have contributed to discrepancies between transports in the model and observations. For instance, surface wind fields differ greatly among different products in the tropical Pacific (e.g., Hackert et al. 2001) and these differences can lead to large differences in patterns and strength of oceanic circulation (McPhaden and Zhang 2002, 2004). Uncertainties in surface buoyancy fluxes are also very large in the tropical Pacific and the specification of these fluxes can affect model results (Wang and McPhaden 2001). In view of these limitations, the model has performed reasonably well in capturing the correct sense of the increased intensity of the circulation in the tropical Pacific from Period 1 to Period 2.

5. Conclusions

The main conclusions from this study are summarized below:

- Consistent with observations, the HYCOM simulation shows a trend toward increasing pycnocline volume transport across the basin from 1992 to 2003. This increase is attributed primarily to changes in the interior ocean pycnocline transports while variability at the western boundary partially compensates that in the interior. However, this partial compensation is not operative at all times and at all latitudes.
- Meridional volume transport convergence anomalies in the model subtropical pycnocline are in quantitative agreement with anomalous volume transports in both the observed and modeled Equatorial Undercurrent, as well as modeled anomalous upwelling into the mixed layer in the eastern tropical Pacific (Table 1).
- Consistent with the increasing circulation intensity, lateral heat transport out of the tropical control volume (defined as the region between 9°N and 9°S, and from the surface to $\sigma_\theta = 25.3$ isopycnal) increases from Period 1 to Period 2, leading to a cooling of the tropical upper ocean despite that net surface heat

flux into the control volume has increased over the same time.

The overall purpose of this study is to shed light on ocean physics that control tropical Pacific responses to imposed surface forcing variability using an eddy-resolving general circulation model. We found that the decadal changes in pycnocline transport convergence, EUC, equatorial upwelling, and SST in the eastern tropical Pacific vary in concert with one another. As such, changes in STCs and the associated lateral heat transport divergence anomalies play a central role in regulating the tropical Pacific climate on decadal time scales.

The ocean-only model used in this study does not allow it to be used to understand ocean–atmosphere interactions, and the eddy-resolving resolution prohibits sensitivity experiments. In particular, we have not addressed how equatorial SST anomalies may influence the atmosphere circulation and, furthermore, how the atmospheric feedbacks may affect STC transports. Coarser-resolution ocean model experiments suggest that both tropical and extratropical wind anomalies can have an impact on the STCs and tropical SST variability on interannual and decadal time scales (Nonaka et al. 2002). These forcing mechanisms are likely to play a role even in eddy-resolving models.

The model and the observations are in qualitative agreement on several key aspects of oceanic variability. But, there are still significant quantitative differences between the modeled interior pycnocline transport values and observations, as discussed earlier. Apparently, our ability to better understand and more accurately simulate the earth's climate and its variations relies on further improvement in the design and implementation of global ocean and atmosphere observation systems, better estimates of air–sea fluxes, and advances in model physics formulations.

REFERENCES

Bleck, R., 2002: An oceanic general circulation model framed in hybrid isopycnic-Cartesian coordinates. *Ocean Modell.,* **4,** 55–88.

——, G. R. Halliwell Jr., A. J. Wallcraft, S. Carroll, K. Kelly, and K. Rushing, cited 2002: Hybrid Coordinate Ocean Model (HYCOM) user's manual: Details of the numerical code. [Available online at http://hycom.rsmas.miami.edu.]

Capotondi, A., M. A. Alexander, C. Deser, and M. J. McPhaden, 2005: Anatomy and decadal evolution of the Pacific subtropical–tropical cells (STCs). *J. Climate,* **18,** 3739–3758.

Carnes, M., 2002: Data base description for the Generalized Digital Environmental Model (GDEM-V)(U), version 3.0. U.S. Naval Oceanographic Office Tech. Rep., 27 pp. [Available from the NAVOCEANO, Oceanographic Data Bases Division, Stennis Space Center, MS 39522–5003.]

Chang, P., B. S. Giese, L. Ji, H. F. Seidel, and F. Wang, 2001: Decadal change in the south tropical Pacific in a global assimilation analysis. *Geophys. Res. Lett.,* **28,** 3461–3464.

Chassignet, E. P., L. T. Smith, G. R. Halliwell, and R. Bleck, 2003: North Atlantic simulations with the Hybrid Coordinate Ocean Model (HYCOM): Impact of the vertical coordinate choice, reference pressure, and thermobaricity. *J. Phys. Oceanogr.,* **33,** 2504–2526.

Davis, R. E., 1976: Predictability of sea surface temperature and sea level pressure anomalies over the North Pacific Ocean. *J. Phys. Oceanogr.,* **6,** 249–266.

Deser, C., M. A. Alexander, and M. S. Timlin, 1996: Upper-ocean thermal variations in the North Pacific during 1970–1991. *J. Climate,* **9,** 1840–1855.

Fedorov, A. V., and S. G. Philander, 2001: A stability analysis of tropical ocean–atmosphere interactions: Bridging measurements and theory for El Niño. *J. Climate,* **14,** 3086–3101.

Fukumori, I., T. Lee, B. Cheng, and D. Benemenlis, 2004: The origin, pathway, and destination of Niño-3 water estimated by a simulated passive tracer and its adjoint. *J. Phys. Oceanogr.,* **34,** 582–604.

Giese, B. S., S. C. Urizar, and N. S. Fučkar, 2002: Southern Hemisphere origins of the 1976 climate shift. *Geophys. Res. Lett.,* **29,** 1014, doi:10.1029/2001GL013268.

Gu, D. F., and S. G. H. Philander, 1997: Interdecadal climate fluctuations that depend on exchanges between the tropics and extratropics. *Science,* **275,** 805–807.

Hackert, E. C., A. J. Busalacchi, and R. Murtugudde, 2001: A wind comparison study using an ocean general circulation model for the 1999–1998 El Nino. *J. Geophys. Res.,* **106,** 2345–2362.

Halliwell, G. R., 2004: Evaluation of vertical coordinate and vertical mixing algorithms in the HYbrid-Coordinate Ocean Model (HYCOM). *Ocean Modell.,* **7,** 285–322.

Hazeleger, W., P. de Vries, and G. J. van Oldenborgh, 2001: Do tropical cells ventilate the Indo-Pacific equatorial thermocline? *Geophys. Res. Lett.,* **28,** 1763–1766.

——, R. Seager, M. A. Cane, and N. H. Naik, 2004: How can tropical Pacific Ocean heat transport vary? *J. Phys. Oceanogr.,* **34,** 320–333.

Huang, R. X., and B. Qiu, 1994: Three-dimensional structure of the wind-driven circulation in the subtropical North Pacific. *J. Phys. Oceanogr.,* **24,** 1608–1622.

——, and ——, 1998: The structure of the wind-driven circulation in the subtropical South Pacific Ocean. *J. Phys. Oceanogr.,* **28,** 1173–1186.

Johnson, G. C., M. J. McPhaden, and E. Firing, 2001: Equatorial Pacific Ocean horizontal velocity, divergence, and upwelling. *J. Phys. Oceanogr.,* **31,** 839–849.

Kara, A. B., P. A. Rochford, and H. E. Hurlburt, 2002: Air-sea flux estimates and the 1997–1998 ENSO event. *Bound.-Layer Meteor.,* **103,** 439–458.

——, A. J. Wallcraft, and H. E. Hurlburt, 2005: A new solar radiation penetration scheme for use in ocean mixed layer studies: An application to the Black Sea using a fine resolution Hybrid Coordinate Ocean Model (HYCOM). *J. Phys. Oceanogr.,* **35,** 13–32.

Kleeman, R., J. P. McCreary, and B. A. Klinger, 1999: A mechanism for generating ENSO decadal variability. *Geophys. Res. Lett.,* **26,** 1743–1746.

Knox, R., and D. Halpern, 1982: Long range Kelvin wave propagation of transport variations in Pacific Ocean equatorial currents. *J. Mar. Res.,* **40** (Suppl.), 329–339.

Large, W. G., J. C. McWilliams, and S. C. Doney, 1994: Oceanic vertical mixing: A review and a model with a nonlocal boundary layer parameterization. *Rev. Geophys.,* **32,** 363–403.

Latif, M., and T. P. Barnett, 1994: Causes of decadal climate variability over the North Pacific and North America. *Science,* **266,** 634–637.

Lee, T., and I. Fukumori, 2003: Interannual-to-decadal variations of tropical–subtropical exchange in the Pacific Ocean: Boundary versus interior pycnocline transports. *J. Climate,* **16,** 4022–4042.

Liu, Z., 1994: A simple model of the mass exchange between the subtropical and tropical ocean. *J. Phys. Oceanogr.,* **24,** 1153–1165.

——, and B. Huang, 2000: Cause of tropical Pacific warming trend. *Geophys. Res. Lett.,* **27,** 1935–1938.

——, S. G. H. Philander, and R. C. Pacanowski, 1994: A GCM study of tropical–subtropical upper-ocean water exchange. *J. Phys. Oceanogr.,* **24,** 2606–2623.

Lu, P., J. P. McCreary, and B. A. Klinger, 1998: Meridional circulation cells and the source waters of the Pacific Equatorial Undercurrent. *J. Phys. Oceanogr.,* **28,** 62–84.

Luyten, J. R., J. Pedlosky, and H. Stommel, 1983: The ventilated thermocline. *J. Phys. Oceanogr.,* **13,** 292–309.

Mantua, N. J., S. R. Hare, Y. Zhang, J. M. Wallace, and R. C. Francis, 1997: A Pacific interdecadal climate oscillation with impacts on salmon production. *Bull. Amer. Meteor. Soc.,* **78,** 1069–1079.

McCreary, J., and P. Lu, 1994: Interaction between the subtropical and equatorial ocean circulation: The subtropical cell. *J. Phys. Oceanogr.,* **24,** 466–497.

McPhaden, M. J., and D. Zhang, 2002: Slowdown of the meridional overturning circulation in the upper Pacific Ocean. *Nature,* **415,** 603–608.

——, and ——, 2004: Pacific Ocean circulation rebounds. *Geophys. Res. Lett.,* **31,** L18301, doi:10.1029/2004GL020727.

——, and Coauthors, 1998: The tropical ocean global atmosphere observing system: A decade of progress. *J. Geophys. Res.,* **103,** 14 169–14 240.

Meinen, C. S., M. J. McPhaden, and G. C. Johnson, 2001: Vertical velocities and transports in the equatorial Pacific during 1993–99. *J. Phys. Oceanogr.,* **31,** 3230–3248.

Merryfield, W. J., and G. J. Boer, 2005: Variability of upper Pacific Ocean overturning in a coupled climate model. *J. Climate,* **18,** 666–683.

National Oceanic and Atmospheric Administration, 1986: ETOP05 digital relief of the surface of the Earth. National Geophysical Data Center Data Announcement 86-MGG-07, 7 pp.

Nonaka, M., S.-P. Xie, and J. P. McCreary, 2002: Decadal variations in the subtropical cells and equatorial pacific SST. *Geophys. Res. Lett.,* **29,** 1116, doi:10.1029/2001GL013717.

Pedlosky, J., 1987: An inertial theory of the equatorial undercurrent. *J. Phys. Oceanogr.,* **17,** 1978–1985.

——, 1988: Entrainment and the termination of the equatorial undercurrent. *J. Phys. Oceanogr.,* **18,** 880–886.

Plimpton, P. E., H. P. Freitag, and M. J. McPhaden, 2004: Processing of subsurface ADCP data in the equatorial Pacific. Pacific Marine Environmental Laboratory, NOAA Tech. Memo. OAR PMEL-125, 41 pp.

Schneider, N., A. J. Miller, M. A. Alexander, and C. Deser, 1999: Subduction of decadal North Pacific temperature anomalies: Observations and dynamics. *J. Phys. Oceanogr.,* **29,** 1056–1070.

Smith, L. T., E. P. Chassignet, and R. Bleck, 2000: The impact of lateral boundary conditions and horizontal resolution on North Atlantic water mass transformations and pathways in an isopycnic coordinate ocean model. *J. Phys. Oceanogr.,* **30,** 137–159.

Smith, W. H. F., and D. T. Sandwell, 1997: Global seafloor topography from satellite altimetry and ship depth soundings. *Science,* **277,** 1956–1962.

Springer, S., M. J. McPhaden, and A. J. Busalacchi, 1990: Oceanic heat content variability in the tropical Pacific during the 1982–83 El Niño. *J. Geophys. Res.,* **95,** 22 089–22 102.

Wang, W., and M. J. McPhaden, 2001: What is the mean seasonal cycle of surface heat flux in the equatorial Pacific? *J. Geophys. Res.,* **106,** 837–857.